Since January 2020 Elsevier has created a COVID-19 resource centre with free information in English and Mandarin on the novel coronavirus COVID-19. The COVID-19 resource centre is hosted on Elsevier Connect, the company's public news and information website.

European Journal of Medicinal Chemistry 240 (2022) 114596

Contents lists available at ScienceDirect

European Journal of Medicinal Chemistry

journal homepage: www.elsevier.com/locate/ejmech

A systematic exploration of boceprevir-based main protease inhibitors as SARS-CoV-2 antivirals

Yugendar R. Alugubelli [a,1], Zhi Zachary Geng [a,1], Kai S. Yang [a,1], Namir Shaabani [b,1], Kaustav Khatua [a,1], Xinyu R. Ma [a,1], Erol C. Vatansever [a,1], Chia-Chuan Cho [a,1], Yuying Ma [a,1], Jing Xiao [a], Lauren R. Blankenship [a], Ge Yu [a], Banumathi Sankaran [c], Pingwei Li [d], Robert Allen [b], Henry Ji [b,**], Shiqing Xu [a,***], Wenshe Ray Liu [a,d,e,f,*]

[a] Texas A&M Drug Discovery Laboratory, Department of Chemistry, Texas A&M University, College Station, TX, 77843, USA
[b] Sorrento Therapeutics, Inc. San Diego, CA, 92121, USA
[c] Molecular Biophysics and Integrated Bioimaging, Berkeley Center for Structural Biology, Laurence Berkeley National Laboratory, Berkeley, CA, 94720, USA
[d] Department of Biochemistry and Biophysics, Texas A&M University, College Station, TX, 77843, USA
[e] Institute of Biosciences and Technology and Department of Translational Medical Sciences, College of Medicine, Texas A&M University, Houston, TX, 77030, USA
[f] Department of Molecular and Cellular Medicine, College of Medicine, Texas A&M University, College Station, TX, 77843, USA

ARTICLE INFO

Keywords:
COVID-19
SARS-CoV-2
Main protease
Covalent inhibitor
Carbamate

ABSTRACT

Boceprevir is an HCV NSP3 inhibitor that was explored as a repurposed drug for COVID-19. It inhibits the SARS-CoV-2 main protease (M^{Pro}) and contains an α-ketoamide warhead, a P1 β-cyclobutylalanyl moiety, a P2 dimethylcyclopropylproline, a P3 *tert*-butylglycine, and a P4 *N*-terminal *tert*-butylcarbamide. By introducing modifications at all four positions, we synthesized 20 boceprevir-based M^{Pro} inhibitors including PF-07321332 and characterized their M^{Pro} inhibition potency in test tubes (*in vitro*) and 293T cells (*in cellulo*). Crystal structures of M^{Pro} bound with 10 inhibitors and cytotoxicity and antiviral potency of 4 inhibitors were characterized as well. Replacing the P1 site with a β-(S-2-oxopyrrolidin-3-yl)-alanyl (Opal) residue and the warhead with an aldehyde leads to high *in vitro* potency. The original moieties at P2, P3 and the P4 *N*-terminal cap positions in boceprevir are better than other tested chemical moieties for high *in vitro* potency. In crystal structures, all inhibitors form a covalent adduct with the M^{Pro} active site cysteine. The P1 Opal residue, P2 dimethylcyclopropylproline and P4 *N*-terminal *tert*-butylcarbamide make strong hydrophobic interactions with M^{Pro}, explaining high *in vitro* potency of inhibitors that contain these moieties. A unique observation was made with an inhibitor that contains a P4 *N*-terminal isovaleramide. In its M^{Pro} complex structure, the P4 *N*-terminal isovaleramide is tucked deep in a small pocket of M^{Pro} that originally recognizes a P4 alanine side chain in a substrate. Although all inhibitors show high *in vitro* potency, they have drastically different *in cellulo* potency to inhibit ectopically expressed M^{Pro} in human 293T cells. In general, inhibitors with a P4 *N*-terminal carbamide or amide have low *in cellulo* potency. This trend is reversed when the P4 *N*-terminal cap is changed to a carbamate. The installation of a P3 *O*-*tert*-butyl-threonine improves *in cellulo* potency. Three molecules that contain a P4 *N*-terminal carbamate were advanced to cytotoxicity tests on 293T cells and antiviral potency tests on three SARS-CoV-2 variants. They all have relatively low cytotoxicity and high antiviral potency with EC_{50} values around 1 μM. A control compound with a nitrile warhead and a P4 *N*-terminal amide has undetectable antiviral potency. Based on all observations, we conclude that a P4 *N*-terminal carbamate in a boceprevir derivative is key for high antiviral potency against SARS-CoV-2.

Abbreviations: COVID-19, coronavirus disease 2019; SARS-CoV-2, severe acute respiratory syndrome coronavirus 2; M^{Pro}, main protease; MPI, main protease inhibitor.

* Corresponding author. Texas A&M Drug Discovery Laboratory, Department of Chemistry, Texas A&M University, College Station, TX, 77843, USA.
** Corresponding author.
*** Corresponding author.
E-mail addresses: hji@sorrentotherapeutics.com (H. Ji), shiqing.xu@tamu.edu (S. Xu), wsliu2007@tamu.edu (W.R. Liu).
[1] Contributed equally to the paper.

https://doi.org/10.1016/j.ejmech.2022.114596
Received 4 May 2022; Received in revised form 29 June 2022; Accepted 5 July 2022
Available online 8 July 2022

1. Introduction

COVID-19 is the currently ongoing pandemic that is caused by the coronavirus SARS-CoV-2. To address this emergency, a large variety of drug repurposing research has been conducted to identify approved medications that might be potentially used as COVID-19 treatments [1–5]. Significant part of this research has been targeting the SARS-CoV-2 main protease (M^{Pro}) [6–12]. M^{Pro} is a peptide fragment of two translation products pp1a and pp1ab of the SARS-CoV-2 RNA genome after the virus infects human cells. Both pp1a and pp1ab are very large polypeptides that need to undergo proteolytic hydrolysis to form 16 nonstructural proteins (nsps). These nsps are essential for the virus to replicate its genome in host cells, evade the host immune system, and package new virions for the infection of new host cells [13]. Intervention of the proteolytic hydrolysis of pp1a and pp1ab is a viable approach to stop SARS-CoV-2 infection. There are two internal peptide fragments from pp1a and pp1b that function as cysteine proteases to hydrolyze all nsps. One is M^{Pro} and the other papain-like protease (PL^{Pro}). As the major protease, M^{Pro} processes the majority of nsps. It is also more conserved than PL^{Pro}. M^{Pro} genes in SARS-CoV and SARS-CoV-2 share 96% sequence identity [2]. Targeting M^{Pro} for drug discovery has been demonstrated as a successful route for the development of SARS-CoV-2 antivirals by the U.S. FDA approval of the emergency use of paxlovid for treating COVID-19 [14]. So far, a number of approved small molecule drugs have been confirmed as potent M^{Pro} inhibitors [1,3,5,6,9–11,15–17]. One of which is boceprevir [15–17]. Boceprevir is a peptidyl inhibitor of HCV NSP3. HCV NSP3 is a serine protease. Boceprevir contains an α-ketoamide warhead that forms a

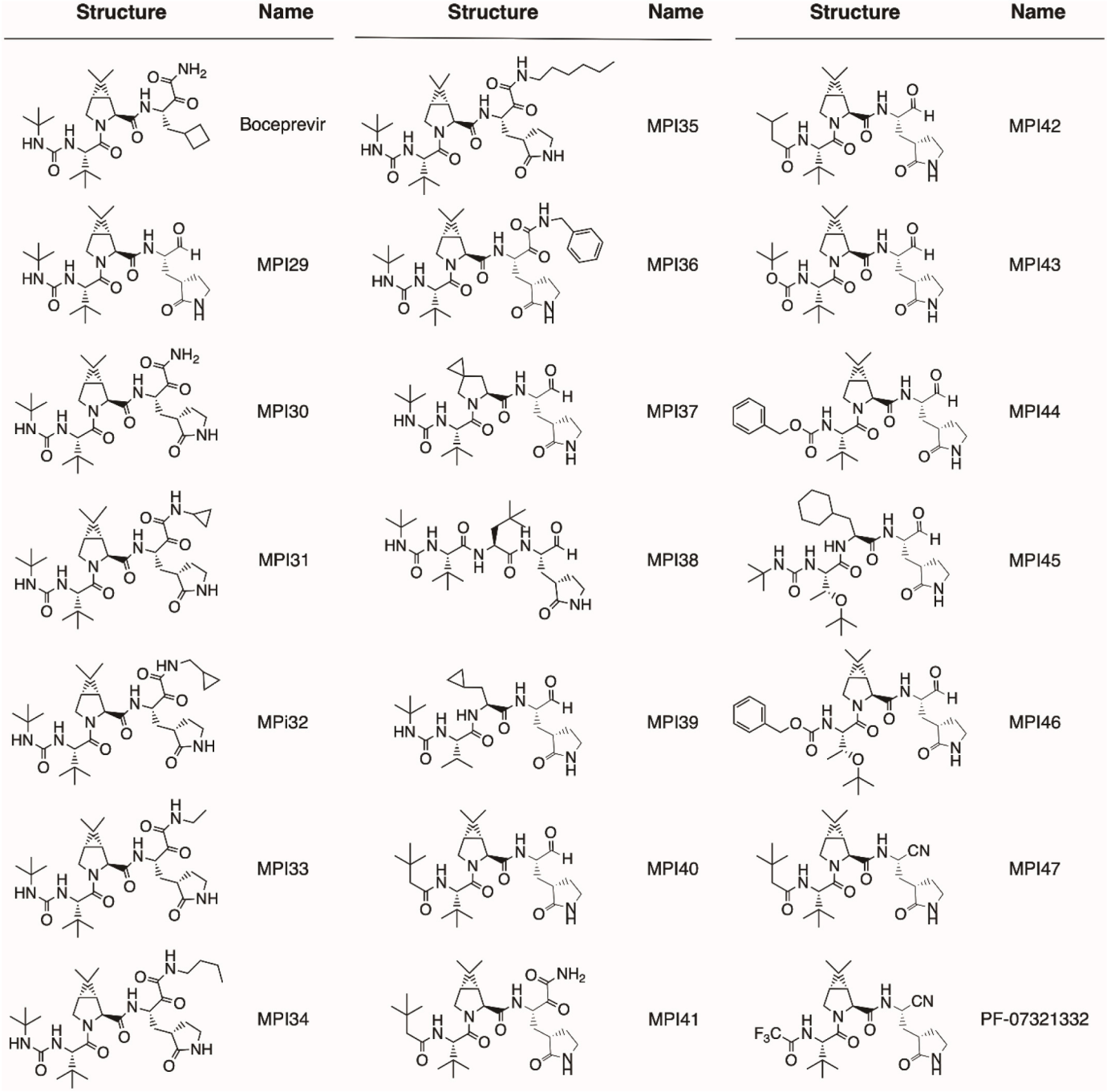

Fig. 1. Structures of boceprevir, MPI29-47 and PF-07321332.

reversible covalent adduct with its active site serine for high inhibition potency [18]. Besides the α-ketoamide warhead, boceprevir contains a P1 β-cyclobutylalanyl moiety, a P2 dimethylcyclopropylproline, a P3 *tert*-butylglycine, and a P4 *N*-terminal *tert*-butylcarbamide. Boceprevir has been shown as a potent inhibitor of M^{Pro} in multiple publications [1, 15–17]. Its interactions with M^{Pro} have also been structurally characterized using X-ray protein crystallography [15–17,19,20]. Although its discovery as a potent M^{Pro} inhibitor created excitement about its potential use as a COVID-19 treatment, boceprevir has moderate antiviral activity against SARS-CoV-2 and displays very low potency to inhibit M^{Pro} in a human cell host [15,16,21]. In this work, we report a systematic study of boceprevir-based molecules for improved cellular and antiviral potency against the SARS-CoV-2 M^{Pro}.

2. Results

2.1. The design and synthesis of MPI29-47 and PF-07321332

In total, we designed 19 boceprevir-based inhibitors as shown in Fig. 1 [22]. Paxlovid is a combination therapy with two components, ritonavir and nirmatrelvir. Nirmatrelvir is an potent M^{Pro} inhibitor and was originally called PF-07321332 [14]. Since it is a boceprevir derivative, we included it in our study as well. M^{Pro} contains four binding pockets in its active site to interact with the P1, P2, P4, and P3' amino acid residues in a substrate [23]. The P1 residue in a substrate is strictly glutamine. Past efforts on the development of M^{Pro} inhibitors have been either using a P1 β-(S-2oxopyrrolidin-3-yl)-alanyl (Opal) residue in a peptidyl inhibitor or a pyridine moiety in a nonpeptidyl inhibitor to engage the S1 (P1 binding) pocket of M^{Pro} for strong interactions [6,8, 16,24–31]. Boceprevir has a P1 β-cyclobutylalanyl moiety that displays loose binding to the M^{Pro} S1 pocket in its M^{Pro} complex structure [15–17, 19,20], which explains its relatively moderate M^{Pro} inhibition potency. In our designed boceprevir derivatives, this site is replaced by the Opal residue. In M^{Pro}-boceprevir complex structures, the P2 dimethylcyclopropylproline binds neatly to the M^{Pro} S2 (P2 binding) pocket. Due to its nice fit to the M^{Pro} S2 pocket, this site is maintained as dimethylcyclopropylproline in most designed inhibitors. In a small number of inhibitors, other residues such as (*S*)-5-azaspiro [2,4]heptane-6-carboxylic acid in MPI37, neopentylglycine in MPI38, β-cyclopropylalanine in MPI39, and cyclohexylalanine in MPI45 at the P2 site are introduced. A previous study has indicated that neopentylglycine, β-cyclopropylalanine and cyclohexylalanine at this site lead to either high M^{Pro} inhibition potency in test tubes (*in vitro*) or in 293T cells that express M^{Pro} (*in cellulo*) [32]. The P3 site is either maintained as *tert*-butylglycine or replaced by *O-tert*-butylthreonine. *tert*-Butylglycine at the P3 site in a peptidyl inhibitor is known to generate high *in vitro* potency and *O-tert*-butylthreonine is known to cause high *in cellulo* and antiviral potency [21,32,33]. Boceprevir has a P4 *N*-terminal *tert*-butylcarbamide cap. This site is either maintained as a carbamide or replaced by a carbamate or amide.

Boceprevir has an α-ketoamide warhead that covalently interacts with the M^{Pro} active site cysteine C145 to generate a hemithioacetal intermediate. Since the majority of currently known peptidyl inhibitors of M^{Pro} have an aldehyde warhead, we replaced the α-ketoamide warhead with an aldehyde in some designed inhibitors. We also tested nitrile at this position since PF-07321332 and some other developed M^{Pro} inhibitors have this warhead [14,34]. An advantage of the α-ketoamide warhead is its allowance of appending additional chemical moieties at its α-ketoamide nitrogen. Both aldehyde- and nitrile-containing inhibitors will leave the M^{Pro} S3' (P3' binding) pocket empty when they bind to M^{Pro}. A chemical appendage at the α-ketoamide nitrogen can potentially reach this pocket for additional interactions and therefore lead to high affinity to M^{Pro}. MPI31-36 were designed for this purpose. The base molecule of MPI31-36 is MPI30 that is different from boceprevir only at the P1 residue. Please note that MPI30 is a previously developed M^{Pro} inhibitor with a name as ML1000, though the structural characterization of its complex with M^{Pro} has not been reported [35]. We follow typical peptide coupling chemistry to synthesize all inhibitors including PF-07321332. In general, the synthesis started from the P4 *N*-terminal cap to the *C*-terminal warhead. All compounds were strictly characterized to ensure their purity. Synthetic details and characterizations are provided in the supplementary information.

2.2. Kinetic characterizations of MPI29-47 and PF-07321332 on their in vitro enzymatic inhibition potency

In a previous drug repurposing project, we established a protocol to characterize M^{Pro} inhibitors [12]. In this protocol, a fluorogenic substrate Sub3 is used. We followed this protocol to characterize *in vitro* M^{Pro} inhibition potency for all synthesized inhibitors by determining their IC_{50} values. To conduct the assay, we preincubated 20 nM M^{Pro} with varied concentrations of an inhibitor for 30 min before 10 μM Sub3 was added and the fluorescent product formation was recorded in a fluorescence plate reader. 30 min incubation time with M^{Pro} is a standard procedure that has been used by multiple labs in the determination of IC_{50} values for M^{Pro} inhibitors [12,16,29,36]. All our designed inhibitors are reversible covalent inhibitors, their incubation times with M^{Pro} are not expected to significantly influence their determined IC_{50} values. As a matter of fact, a previous IC_{50} analysis in which MPI11 was incubated with M^{Pro} for three different times led to very similar characterized IC_{50} values [32]. For MPI29-47 and PF-07321332, they all exhibited well defined inhibition curves that started from 100% activity without an inhibitor and reached to almost total inhibition when 10 μM of an inhibitor was provided. Data are presented in Fig. 2. We fit all collected data to a four-parameter variable slope inhibition equation in GraphPad 9.0 to obtain IC_{50} values for all inhibitors. Determined IC_{50} values are presented in Table 1. As shown in Table 1, MPI29 has the highest *in vitro* potency with an IC_{50} value as 9.3 nM. Since we used 20 nM M^{Pro} for the assay, this IC_{50} value has reached the detection limit. Real *in vitro* potency of MPI29 is likely higher than what the determined IC_{50} value indicates. MPI29 has an aldehyde warhead. MPI30 is different from MPI29 only at the warhead position. It has an α-ketoamide instead. MPI30 has a determined IC_{50} value as 40 nM. This value is similar to that reported by Westberg et al. [35]. This lower potency than MPI29 is expected since α-ketoamide is less chemically reactive than aldehyde toward a nucleophile. However, MPI30 is 100-fold more potent than boceprevir indicating the essential role of the P1 Opal residue in improving interactions with M^{Pro}. MPI31-36 all have much higher *in vitro* IC_{50} values than MPI30. Apparently adding a chemical appendage to the α-ketoamide nitrogen leads to less favorable interactions with M^{Pro}. Interestingly, MPI33 that has the smallest appendage has an *in vitro* IC_{50} value closest to MPI30. Although the benzyl appendage in MPI36 is bigger than that in MPI32-35, it is less detrimental to the *in vitro* potency indicating that the benzyl group possibly involves some favorable interactions with M^{Pro} in comparison to other *N*-substituents.

MPI37 is different from MPI29 at the P2 residue. It has a determined *in vitro* IC_{50} value as 23 nM. Although replacing the P2 dimethylcyclopropylproline with (*S*)-5-azaspiro [2,4]heptane-6-carboxylic acid leads to less favorable interactions with M^{Pro}, the effect is not dramatic. A similar observation was made with MPI38 that has a P2 neopentylglycine. MPI39 has both P2 and P3 sites different from MPI29. Both residues in MPI39 have been shown in a previous study to favor interactions with M^{Pro} [32]. Accordingly, we notice that MPI39 has relatively high *in vitro* potency. MPI40, MPI42 and MPI43 are different from MPI29 only in their P4 *N*-terminal cap. MPI40 has a P4 *N*-terminal amide that is different from MPI29 only at one atom position. However, this slight change leads to about 20-fold loss of *in vitro* potency. Intriguingly, removing one methyl group from the P4 *N*-terminal cap of MPI40, which leads to MPI42, improves *in vitro* potency for about 9 folds. Another interesting observation is on MPI43. MPI43 has a P4 *N*-terminal carbamate and is different from MPI29 and MPI40 only at the

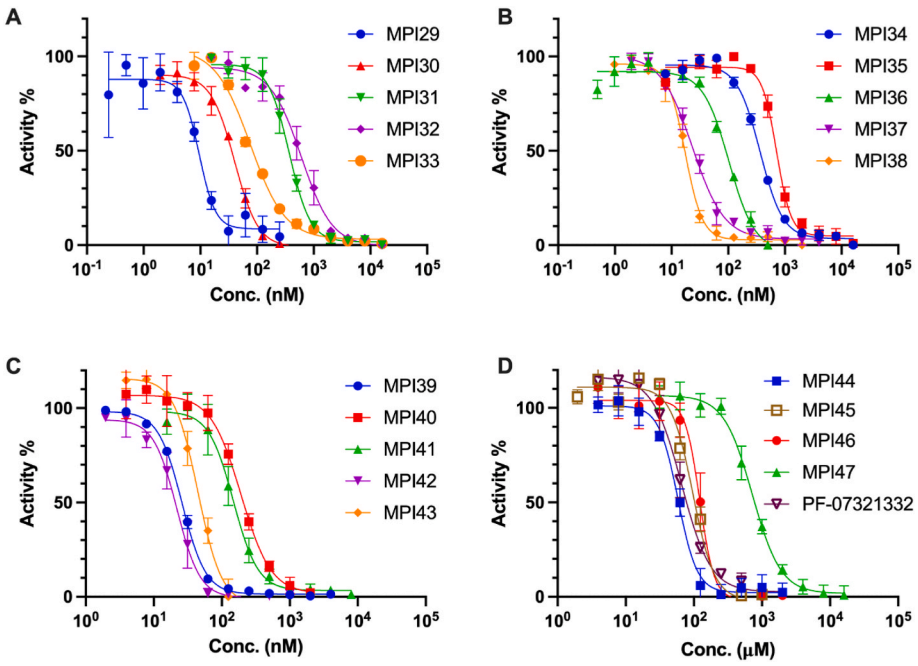

Fig. 2. Inhibition curves of MPI29-47 and PF-07321332 on M^{Pro}. Triplicate experiments were performed for each compound. For all experiments, 20 nM M^{Pro} was incubated with an inhibitor for 30 min before 10 μM Sub3 was added. The M^{Pro}-catalyzed Sub3 hydrolysis rate was determined by measuring linear increase of product fluorescence (Ex: 336 nm/Em: 455 nm) at the initial 5 min reaction time.

Table 1
Determined enzymatic IC_{50}, cellular EC_{50}, and antiviral EC_{50} values of M^{Pro} inhibitors.

Compound ID	Enzymatic IC_{50} (nM)	Cellular EC_{50} (μM)	Antiviral EC_{50} (μM)	PDB Entry	Compound ID	Enzymatic IC_{50} (nM)	Cellular EC_{50} (μM)	Antiviral EC_{50} (μM)	CC_{50} (μM)	PDB Entry
Boceprevir	4200 ± 600 [16]/8000 ± 1500 [15]	>10			MPI39	26 ± 1	>10			
MPI29	9.3 ± 0.8	>5		7S6W	MPI40	180 ± 20	7.4 ± 0.9	n.d.[a]/n.d.[b]/n.d.[c]		
MPI30	40 ± 4	>10		7S6X	MPI41	150 ± 20	7.7 ± 1.5			
MPI31	360 ± 50	>10			MPI42	22 ± 4	2.6 ± 0.5			7S75
MPI32	620 ± 170	>10		7S6Y	MPI43	45 ± 5	0.37 ± 0.04	0.61[a]/0.36[b]/1.00[c]	34.2	
MPI33	75 ± 9	>10		7S6Z	MPI44	59 ± 7	0.31 ± 0.03	2.94[a]/0.86[b]/1.04[c]	143.7	
MPI34	370 ± 30	>10		7S70	MPI45	97 ± 11	0.74 ± 0.11			
MPI35	720 ± 80	>5		7S71	MPI46	120 ± 10	0.14 ± 0.02	1.08[a]/2.28[b]/0.75[c]	163.4	
MPI36	102 ± 2	>10		7S72	MPI47	720 ± 90	>10			
MPI37	23 ± 1	>10		7S73	PF-07321332	66 ± 12	3.4 ± 0.8	1.30		
MPI38	17 ± 2	>5		7S74						

n.d.: no detectable value.
[a] Antiviral EC_{50} value for the USA-WA1/2020 strain.
[b] Antiviral EC_{50} value for the Beta strain.
[c] Antiviral EC_{50} value for the Delta strain.

carbamate oxygen position. It has *in vitro* potency between MPI29 and MPI40. Therefore, switching a P4 *N*-terminal carbamide nitrogen to oxygen is less detrimental to *in vitro* potency than switching it to methylene. MPI41 is an α-ketoamide derivative of MPI40. It has *in vitro* potency surprisingly similar to MPI40 although α-ketoamide is expected to be less reactive than aldehyde. MPI44 is different from MPI43 at its P4 *N*-terminal *O*-alkyl group. It has a benzyl group instead of a *tert*-butyl group as in MPI43. Although two *O*-alkyl groups are structurally different, MPI43 and MPI44 have similar *in vitro* potency. In our previous work, we noticed that an *O*-benzyl group at this position loosely binds M^{Pro} [32,33]. Similar *in vitro* potency between MPI43 and MPI44 indicates that an *O-tert*-butyl group at this position might involve loose interactions with M^{Pro} as well. In our previous work, we discovered that MPI8, a peptidyl aldehyde has the highest *in cellulo* and antiviral potency among all inhibitors that we synthesized [21]. Due to the high *in vitro* potency of MPI29, we created chimera inhibitors MPI45 and MPI46 that integrate structural components from both MPI8 and MPI29. MPI45 is a chimera in which the P4 *N*-terminal cap of MPI29 is fused to the rest of MPI8 and MPI46 is a product made by switching the P2 residue in MPI8 to the one in MPI29. Both MPI45 and MPI46 have *in vitro* potency similar to MPI8 with an IC_{50} value about 100 nM [33]. MPI47 is different from MPI40 only at its warhead. It has an *in vitro* IC_{50} value as 720 nM. Apparently switching the warhead to nitrile from either aldehyde or α-ketoamide leads to significant loss of *in vitro* potency. Although

PF-07321332 and MPI47 are structurally similar, PF-07321332 has a more than 10-folder lower IC_{50} value than MPI47. A likely explanation is that the P4 N-terminal trifluoroacetamide cap in PF-07321332 involves unique interactions with M^{Pro} that do not exist for MPI47, which is supported by the crystal structure of M^{Pro} bound with PF-07321332 [14, 37,38].

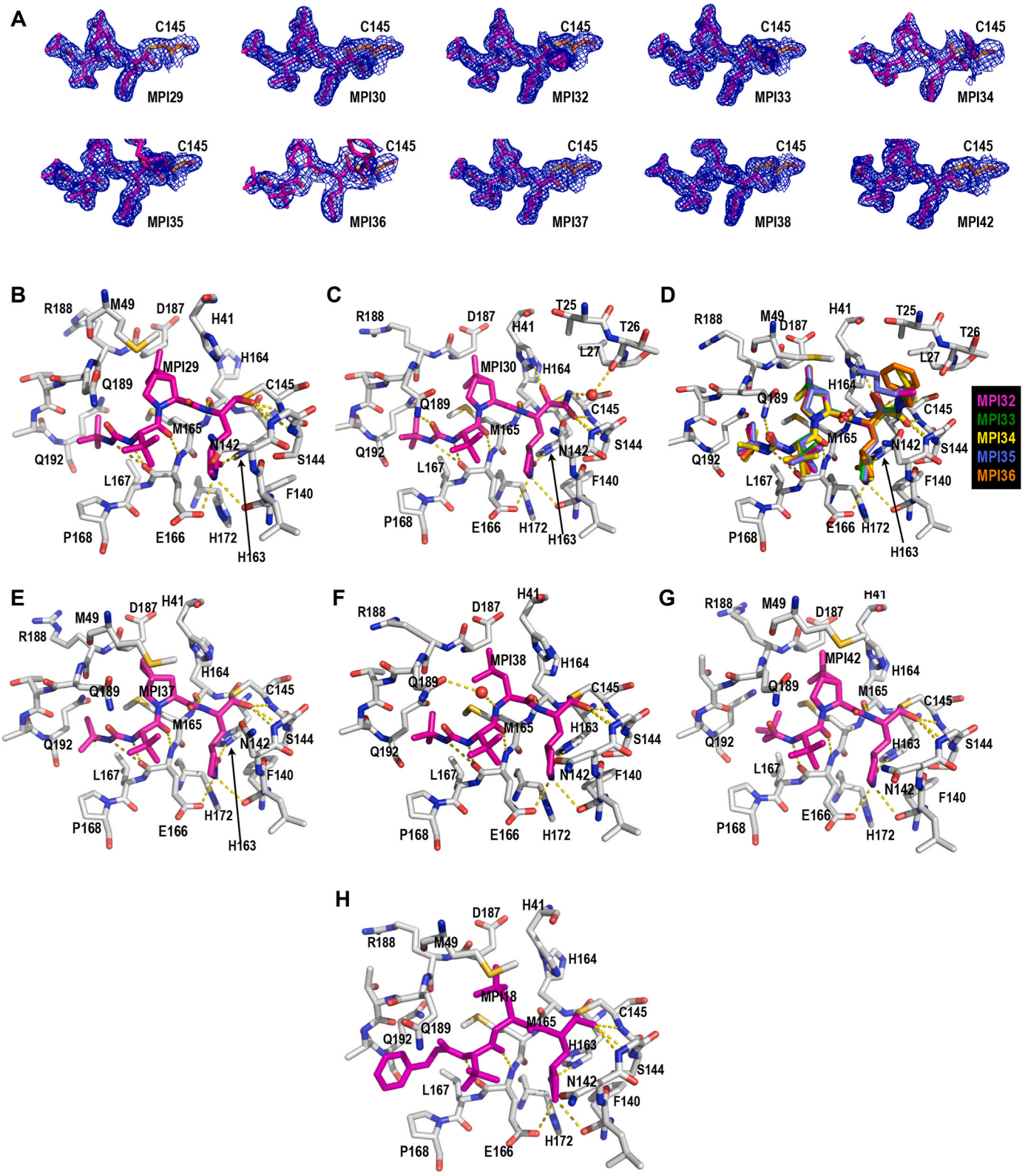

Fig. 3. Crystal structures of M^{Pro} bound with 10 inhibitors. (A): Contoured $2F_o$-F_c maps at the 1σ level around 10 MPIs and C145 in the active site of M^{Pro}. (B–G): The active site structures for M^{Pro} bound with (B) MPI29, (C) MPI30, (D) MPI32-MPI36, € MPI37, (F) MPI38, (G) MPI42, and (H) MPI8. The structure of MPI18 is based on the PDB entry 7RVR. It is provided as a comparison. Dashed yellow lines between inhibitors and M^{Pro} are hydrogen bonds.

2.3. X-ray crystallography analysis of M^{Pro} bound with 10 inhibitors

In order to structurally characterize our developed inhibitors in their complexes with M^{Pro}. We crystalized M^{Pro} in its apo form and then soaked obtained crystals with our designed inhibitors for X-ray crystallography analysis. Using this approach, we successfully determined 10 M^{Pro}-inhibitor complex structures to high resolutions. These inhibitors include MPI29, MPI30, MPI32-38, and MPI42. PDB entries for these M^{Pro}-inhibitor complex structures are summarized in Table 1. In the active sites of all M^{Pro}-inhibitor complexes, electron density is well shaped for unambiguous modeling of inhibitors except for MPI36 at its α-ketoamide *N*-benzyl group (Fig. 3A). A covalent bond between C145 of M^{Pro} and the warhead of an inhibitor is clearly visible in all structures. MPI29, MPI37, MPI38, and MPI42 have an aldehyde warhead. In the M^{Pro}-MPI29 complex as shown in Fig. 3B, MPI29 forms a number of hydrogen bonds with M^{Pro}. The amide of the P1 Opal side chain lactam forms three hydrogen bonds with M^{Pro} residues including F140 at its backbone oxygen, H163 at one of its imidazole nitrogen atoms and E166 at its side chain carboxylate. These three hydrogen bonds have also been observed in structures of M^{Pro} bound with other inhibitors containing a P1 Opal side chain lactam. There are two hydrogen bonds generated between two backbone amides of MPI29 and M^{Pro} residues including H164 at its backbone oxygen and E166 at its backbone nitrogen. Similar hydrogen bonds have been observed in structures of M^{Pro} bound with other peptidyl inhibitors. The P4 *N*-terminal carbamide cap of MPI29 uses its two nitrogen atoms to form hydrogen bonds with the backbone oxygen of M^{Pro} E166. In previously published structures of M^{Pro} bound with peptidyl aldehyde inhibitors that have a P4 *N*-terminal carbamate, typically only one hydrogen bond is observed between the P4 *N*-terminal cap and M^{Pro} E166. One additional hydrogen bond that is formed between the P4 *N*-terminal cap and M^{Pro} E166 provides an explanation of very high *in vitro* potency of MPI29. Since the introduction a carbamide nitrogen causes binding energy loss due to desolvation, this energy loss is apparently counteracted possibly by this additional hydrogen bond formed between MPI29 and M^{Pro}. In the M^{Pro}-MPI29 complex, the hemithioacetal hydroxide is predominantly in an *S* configuration and poises to interact with three M^{Pro} backbone amide NH groups from G143, S144 and C145 that purportedly generate an oxyanion hole to stabilize the transition state of M^{Pro}-catalyzed hydrolysis of a substrate. This favorable binding of the hemithioacetal hydroxide at the oxyanion hole likely contributes to strong *in vitro* potency for peptidyl aldehyde inhibitors. It is debating that whether the hemithioacetal hydroxide is at its deprotonated and therefore charged form. Since a hemithioacetal hydroxide has a much lower pKa value than a regular alcohol and the site prefers a negatively charged hydroxide, it is highly likely that the hemithioacetal hydroxide is negatively charged. If this is the situation, one may generally bear in mind to introduce a negatively charged moiety in a designed inhibitor to bind to this anion hole in M^{Pro} for improved affinity. In M^{Pro}-MPI29, the P2 dimethylcyclopropylproline is in van der Waals distances to most surrounding M^{Pro} residues in the S2 pocket, which indicates favorable hydrophobic interactions. Based on the structure, there is not much space left for adding additional chemical moieties into the inhibitor to improve affinity. However, the plasticity of M^{Pro} may allow the change around the S2 pocket to accommodate even large P2 residues in inhibitors. The P3 *tert*-butylglycine is in the van der Waals distance to the side chain of M^{Pro} E166 but apparently doesn't engage other residues in M^{Pro}. This is known in most peptidyl inhibitors for M^{Pro}. However, the *tert*-butyl group in the P4 *N*-terminal cap fits nicely to the M^{Pro} P4 binding pocket indicating favorable van der Waals interactions with surrounding M^{Pro} residues. All these favorable interactions likely contribute to the exceedingly high *in vitro* potency of MPI29. In previously published structures of M^{Pro} bound with peptidyl inhibitors that contained a P4 *N*-terminal benzoxycarbonyl (CBZ) group such as the M^{Pro}-MPI18 structure shown in Fig. 3H, the CBZ group was typically not structurally defined [32,33,39]. It is apparent that the *tert*-butyl carbamide fits better than the CBZ group to the S4 pocket of M^{Pro}.

MPI30 is different from MPI29 only at its warhead. It has an α-ketoamide. In its crystal structure as shown in Fig. 3C, MPI30 forms interactions with M^{Pro} similar to MPI29 at the P1, P2 and P3 residues and the P4 *N*-terminal group. We observed one additional hydrogen bond that is formed between the P4 *N*-terminal carbamide oxygen and the side chain of M^{Pro} Q189. Q189 is a residue that adopts different conformations in reported structures. Given that its hydrogen bonding interactions with an inhibitor may improve the inhibitor selectivity over other proteins, one may take advantage of this aspect to design M^{Pro} inhibitors. The keto group of the α-ketoamide of MPI30 covalently interacts with M^{Pro} C145 to generate a hemithioacetal. Unlike MPI29, the hemithioacetal hydroxide adopts a conformation pointing away from the oxyanion hole. It is in an unambiguously *S* configuration and interacts with H41 through two water-bridged hydrogen bonds. The amide part of the warhead points toward the oxyanion hole. The amide oxygen is assigned at the oxyanion hole due to its ability to form hydrogen bonds with three backbone NH groups from M^{Pro}. The amide nitrogen interacts indirectly with the backbone oxygen of M^{Pro} T26 through two water-bridged hydrogen bonds. All these interactions likely contribute to the high *in vitro* potency of MPI30. As aforementioned, aldehyde-based inhibitors potentially generate a negatively charged hemithioacetal hydroxide to potently bind the M^{Pro} anion hole. Give that the hemithioacetal hydroxide points away from the anion hole in the M^{Pro}-MPI30 structure, this potential strong interaction is lost. The α-ketoamide is also expected to react with the M^{Pro} active site cysteine much weaker than the aldehyde warhead. Apparently both weakening effects are counterbalanced by additional interactions that are generated between M^{Pro} and the MPI30 α-ketoamide.

Since MPI32-36 have an MPI30 base structure and different *N*-appendages on the α-ketoamide, they are presented together in Fig. 3D. Except at the appendage position, all other parts of MPI32-36 interact with M^{Pro} similar to MPI30. We designed MPI32-36 with a hope that their α-ketoamide *N*-appendages may reach the M^{Pro} S3′ pocket for favorable interactions. However, all *N*-appendages have a *Z* configuration that is energetically favorable and consequently makes them point away from the M^{Pro} S3′ pocket. The appendage of MPI35 is long enough to fold back to the M^{Pro} S3' pocket. Since the *N*-benzyl group of MPI36 has weak electron density around the phenyl ring, it is difficult to assess its interactions with M^{Pro}. Its more favorable *in vitro* potency than MPI34 and MPI35 is likely due to higher structural rigidity of the *N*-benzyl group than two flexible *N*-alkyl groups in MPI34 and MPI35. The indirect interaction between the α-ketoamide nitrogen and M^{Pro} T26 that was observed in the M^{Pro}-MPI30 structure is not observed in M^{Pro} complexes with MPI32-36. All *N*-appendages occupy the original water position and consequently remove interactions involving this water molecule. This might contribute to low *in vitro* potency of MPI32-36. Other *N*-aromatic functionalities and modifications to the *N*-benzyl group may be introduced to MPI36 to improve the binding to M^{Pro}. However, delicate tuning will be necessary.

As shown in Fig. 3E and F, MPI37 and MPI38 interact with M^{Pro} similar to MPI29. The P2 residue in MPI37 occupies slightly less space than that in MPI29. This may contribute to less *in vitro* potency of MPI37 than MPI29. In M^{Pro}-MPI38, there exists a water molecule that bridges an indirect interaction between the P2 backbone nitrogen and the side chain of M^{Pro} Q189. MPI38 displays an M^{Pro} binding mode very similar to MPI18 that was previously developed and structurally resolved in its complex with M^{Pro} (PDB entry: 7RVR and Fig. 3H) [32]. The only difference is at the P4 *N*-terminal cap. MPI18 has a P4 *N*-terminal CBZ group that displays loose binding to M^{Pro} and cannot be unambiguously refined in its M^{Pro} complex structure. However, MPI38 has an *N*-*tert*-butylcarbamide cap whose structure can be clearly refined in the M^{Pro}-MPI38 complex. MPI38 is slightly more potent than MPI18. This slightly higher potency might be attributed to more favorable interactions between the P4 *N*-terminal cap and the M^{Pro} P4 binding pocket. Another noticeable difference is at Q189. The side chain of Q189

adopted two different conformations in the two structures. As discussed previously, Q189 is a relatively flexible residue that has shown very different structural modes in M^{Pro}-inhibitor complexes.

MPI42 is structurally similar to MPI29 except that it has a P4 *N*-terminal isovaleramide. As shown in Fig. 3G, MPI42 interacts with M^{Pro} similar to MPI29 except at the P4 *N*-terminal cap. The isovaleramide cap adopts a unique orientation that points deep into the M^{Pro} S4 pocket. This is different from most currently known peptidyl aldehyde inhibitors. M^{Pro} naturally prefers a P4 valine in its substrates. Isovaleramide is almost structurally identical to valine except that it doesn't have an α-amine. It is apparent that isovaleramide engages favorable interactions with M^{Pro} by binding deep to the M^{Pro} P4 binding pocket. This explains its much higher *in vitro* potency than MPI40 that has an additional methyl group at the P4 *N*-terminal cap. The 3,3-dimethylbutamide cap in MPI40 is too bulky to fit into the relatively small M^{Pro} S4 pocket. Due to the high potency induced by this small isovaleramide cap, it is suggested to be incorporated into future inhibitor designs for improved affinity toward M^{Pro}.

2.4. Characterizations of in cellulo M^{Pro} inhibition potency of MPI29-47 and PF-07321332

When expressed in a human cell host, M^{Pro} leads to acute cytotoxicity and drives the host cell to undergo apoptosis. Using this unique feature, we previously developed a cell-based assay to characterize *in cellulo* potency of M^{Pro} inhibitors [21]. In this assay, an inhibitor with *in cellulo* potency suppresses cytotoxicity from an M^{Pro}-eGFP (enhanced green fluorescent protein) fusion protein that is ectopically expressed in 293T cells and consequently leads to host cell survival and enhanced overall expression of M^{Pro}-eGFP that can be characterized by flow cytometry. We consider that this assay is more advantageous over a direct antiviral assay in the characterization of M^{Pro} inhibitors since an inhibitor may block functions of host proteases such as TMPRSS2, furin, and cathepsin L that are critical for SARS-CoV-2 infection and therefore provides false positive *in cellulo* potency results for M^{Pro} inhibitors [40–42]. False positive results from targeting TMPRSS2, furin, and cathepsin L will lead to wrong structure-activity relationship studies of M^{Pro} inhibitors. Using this novel cellular assay, we characterized a number of repurposed drugs for M^{Pro} inhibitors. Our results indicated that some of these inhibitors suppress SARS-CoV-2 via mechanisms different from M^{Pro} inhibition [21]. Using this novel cellular assay, we characterized all synthesized inhibitors in this work. Inhibitor-driven M^{Pro}-eGFP expression data are presented in Fig. 4 and the determined *in cellulo* EC_{50} values are summarized in Table 1. MPI29-39 that have a P4 *N*-terminal carbamide cap all showed low *in cellulo* potency. Since data for all these inhibitors do not reach a plateau at their highest tested concentrations, their EC_{50} values can only be estimated as higher than 5 or 10 μM. Although MPI29 has the most *in vitro* potency among all inhibitors that we synthesized, it has very weak potency in cells. MPI40-42 have a P4 *N*-terminal amide cap. In comparison to MPI29-39, they showed higher *in cellulo* potency. Their determined EC_{50} values are in a single digit μM range. MPI43 has a P4 *N*-terminal carbamate and is different from MPI29 and MPI40 at only one atom position. It has a determined *in cellulo* EC_{50} value as 0.37 μM. This *in cellulo* potency is 20-fold higher than MPI40 and 160-fold higher than MPI29. Considering that MPI29, MPI40 and MPI43 are different only at one atom position and MPI29 has much higher *in vitro* potency than MPI43, their drastically reversed potency in cells is intriguing. These three inhibitors must have very different plasma/cellular stability, cellular permeability, or both. MPI44 has a P4 *N*-terminal CBZ cap. It has a determined *in cellulo* EC_{50} value similar to that of MPI43. Since MPI43 and MPI44 have similar *in vitro* potency as well, the identity of a P4 *N*-terminal carbamate seems to have little effect on an inhibitor's *in vitro* and *in cellulo* potency. MPI45 and MPI46 each have chemical moieties at two positions that are switched from that in MPI29 to that in MPI8. Both have high *in cellulo* potency. Their determined EC_{50} values are 0.74 and 0.14 μM respectively. It is evident that chemical moieties in MPI8 are optimal for high *in cellulo* potency. The *in cellulo* potency of MPI45 is much lower than that of MPI46 likely due to its P4 *N*-terminal carbamide cap. MPI47 have a P4 *N*-terminal amide. Its determined *in cellulo* EC_{50} value is similar to that for MPI40-42 that also contains a P4 *N*-terminal amide. All four compounds have relatively low cellular potency. PF-07321332 has a determined *in cellulo* EC_{50} value as 3.4 μM. Its better *in cellulo* potency than other inhibitors with an *N*-terminal amide is likely due to its *N*-terminal trifluoro group that may protect the *N*-terminal amide from hydrolysis and/or facilitate the permeability into cells. PF-07321332 was previously shown with an antiviral EC_{50} value

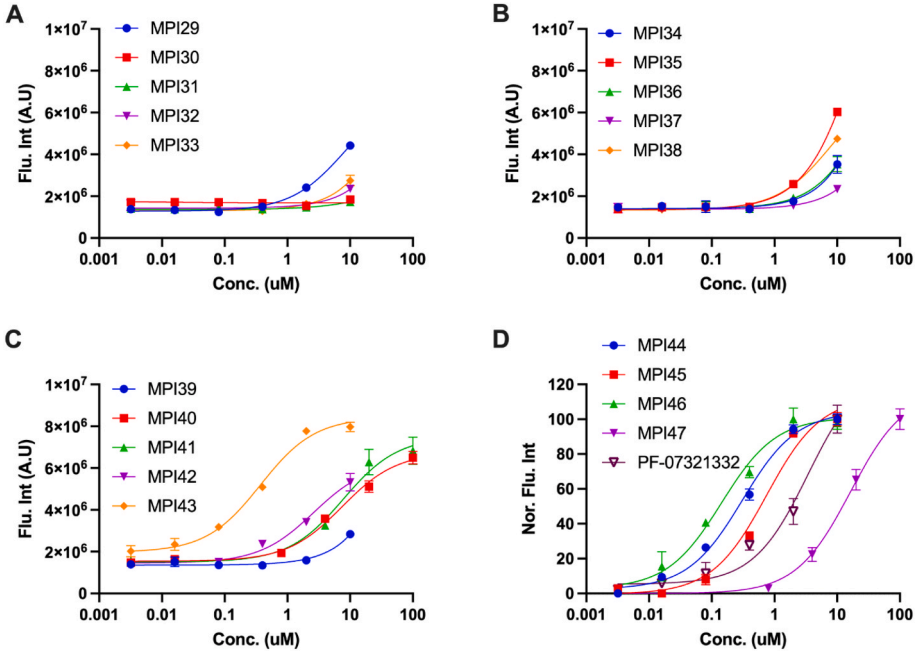

Fig. 4. Cellular potency of MPI29-47 in their inhibition of M^{Pro} to drive host 293T cell survival and overall M^{Pro}-eGFP expression. In D, fluorescent intensity is normalized due to that data for PF-07321332 was collected at a different time using different setups.

as 78 nM to inhibit SARS-CoV-2 in infecting ACE2^{+} A549 cells [14]. Please note that both different cells and different systems were used in this analysis. Direct comparison of the antiviral EC_{50} value from this study to the *in cellulo* EC_{50} value determined in our study is not meaningful. Multiple reasons likely contribute to the discrepancy.

2.5. Characterizations of antiviral potency and cytotoxicity of four selected inhibitors on three SARS-CoV-2 variants

Three most cellularly potent inhibitors MPI43, MPI44 and MPI46 were advanced to antiviral assays. One inhibitor MPI40 that has low cellular potency was characterized as well as a negative control. To quantify their antiviral EC_{50} values, we conducted plaque reduction neutralization tests of three SARS-CoV-2 variants including USA-WA1/2020, Beta and Delta in Vero E6 cells for all four inhibitors. We infected Vero E6 cells by virus in the presence of an inhibitor at various concentrations for three days and then quantified viral plaque reduction. Based on viral plaque reduction data, we determined antiviral EC_{50} values for all inhibitors. MPI40 showed no inhibition at all tested concentrations, which matches its detected low *in cellulo* potency. All other three inhibitors have high antiviral potency. Their determined antiviral EC_{50} values are similar and around 1 μM (Fig. 5 and Table 1). MPI46 shows the most well shaped antiviral data. It inhibits the Delta variants slightly better than the other two SARS-CoV-2 variants. A similar assay of PF-07321332 in its inhibition of USA-WA1/2020 in Vero R6 cells led to a determined antiviral EC_{50} value as 1.3 μM (Supplementary Fig. S1). Please note that the determined antiviral EC_{50} value for PF-07321332 as 75 nM in Vero E6 cells was obtained by the combination use of 2 mM CP-100356 that is an inhibitor of the prototypical ABC transporter [14]. In our study, CP-100356 was not used in all the compounds tested.

We have also characterized cytotoxicity for MPI43, MPI44 and MPI46 in 293T cells using the MTT assay [43]. Cytotoxicity curves of these inhibitors are shown in Supplementary Fig. S2. Determined CC_{50} values are 34.2, 143.7 and 163.4 μM for MPI43, MPI44 and MPI46, respectively. In term of selectivity index (CC_{50}/antiviral EC_{50}), MPI43, MPI44 and MPI46 range from 56 to 233.

3. Discussion

As a potential repurposed drug for COVID-19, boceprevir provided a high hope during the early phase of the COVID-19 pandemic. However, it is only moderate against SARS-CoV-2. Although it shows inhibition of M^{Pro}, it has very weak potency to inhibit M^{Pro} in a human cell host [21]. Lin et al. made ML1000 (MPI30 in our series) based on boceprevir. Although it showed high *in vitro* potency, its antiviral potency was minimal [35]. In our study, both MPI29 and MPI30 are highly potent M^{Pro} inhibitors *in vitro*. The *in vitro* potency of MPI29 has even reached the detection limit of our kinetic assay. However, both inhibitors show very low *in cellulo* potency. Except MPI45 that has some MPI8 moieties, all other inhibitors that have a P4 *N*-terminal carbamide cap all display low *in cellulo* potency. Based on these data, we can conclude that M^{Pro} inhibitors that have a P4 *N*-terminal carbamide will have low cellular and antiviral potency. Although reasons for this low cellular and antiviral potency need to be further investigated, the emergency of COVID-19 demands to focus on other routes to develop M^{Pro} inhibitors as potential SARS-CoV-2 therapeutics.

An alternative to the P4 *N*-terminal carbamide is amide. We synthesized several inhibitors that contain a P4 *N*-terminal amide. In comparison to inhibitors that have a P4 *N*-terminal carbamide, P4 amide-containing inhibitors are relatively more potent in cells but their cellular potency is moderate. In comparison to P4 amide-containing inhibitors that we designed, PF-07321332 that has an *N*-terminal trifluoroacetamide is much more potent in cells. It is highly possible that the bulky trifluoroacetyl group protects the *N*-terminal trifluoroacetamide of PF-07321332 from degradation, a situation that does not exist for other P4 amide-containing inhibitors that we generated. It is also possible the trifluoroacetyl group assists cellular permeability of PF-07321332. Unlike inhibitors with a P4 *N*-terminal carbamide, all three inhibitors with a P4 *N*-terminal carbamate show high cellular potency and also high antiviral potency. These three inhibitors have also low

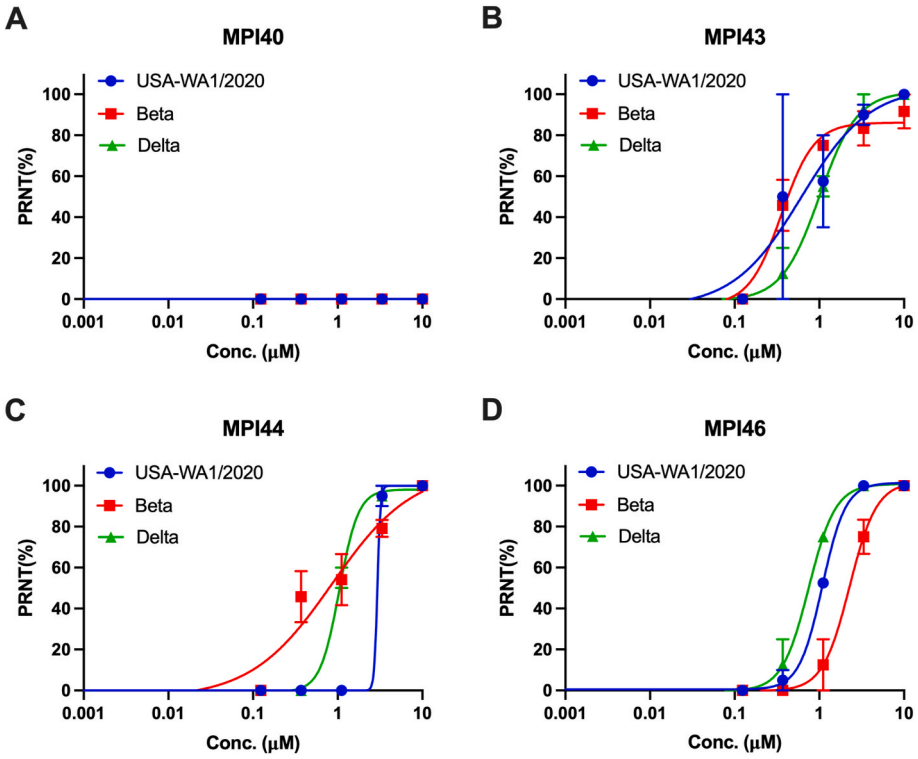

Fig. 5. Plaque reduction neutralization tests (PRNTs) of MPI40, MPI43, MPI44, and MPI46 on their inhibition of three SARS-CoV-2 strains USA-WA1/2020, Beta and Delta in Vero E6 cells. Two repeats were conducted for each concentration.

cytotoxicity. Our collected data support a conclusion that a P4 *N*-terminal carbamate in a boceprevir-based M^{Pro} inhibitor is key for high cellular and antiviral potency.

In other positions, a P1 Opal residue, a P2 dimethylcyclopropylproline, and a P3 *tert*-butylglyine or *O-tert*-butylthreonine are optimal for high cellular and antiviral potency. In previous work, we discovered that a P3 *O-tert*-butylthreonine is critical for an M^{Pro} inhibitor to have high cellular and antiviral potency [32]. This observation is supported by the high cellular and antiviral potency of MPI46. MPI8 was previously discovered as a highly potent SARS-CoV-2 inhibitor with an EC_{50} value as 30 nM [21,33,39]. All boceprevir-based inhibitors that we developed in this work do not reach the potency of MPI8. To improve cellular and antiviral potency of inhibitors such as MPI43, MPI44 and MPI46, a possible route is to search for alternative *O*-alkyl groups in the P4 *N*-terminal carbamate cap for improved binding to the M^{Pro} P4 binding pocket.

For the warhead, all current data indicate that aldehyde has the best activity. Changing it to either α-ketoamide or nitrile significantly decreases both *in vitro* and *in cellulo* potency of an inhibitor. Compounds with an aldehyde will lead to a concern of cytotoxicity. Cytotoxicity and potency of an aldehyde inhibitor for M^{Pro} need to be carefully balanced when it is finally applied in animals or human patients. Pharmacokinetic (PK)/pharmacodynamic (PD) features will also need to be considered. Most currently reported M^{Pro} inhibitors do not have PK/PD results in animals available. We recently characterized MPI8 PK results in rats [44]. MPI8 displayed a relatively quick clearance rate in rats with a half-life as 1.22 h by oral administration. However, PK results for PF-07321322 have shown that it is stable in animals, although it is metabolized by CYP3A4 in humans [14]. The nitrile warhead and other structural moieties likely contribute to this high stability. Since PF-07321332 is a component of an approved drug for COVID-19 already, combining characteristics within PF-07321332 such as the nitrile warhead that has low cytotoxicity concern and that from other boceprevir and/or MPI8-based inhibitors including MPI43, MPI44 and MPI46 for improved PK/PD features need to be explored. PF-07321332 requires to be used together with ritonavir due to its metabolic instability. Strong side effects from ritonavir and serious and sometimes fatal drug interactions between ritonavir and other medications have been reported [45–49]. An obvious drug development goal is to develop a PF-07321332-based SARS-CoV-2 antiviral that will not require the combination use with ritonavir. The metabolization weak point of PF-07321332 is at the P1 Opal side chain lactam. Changing this site to other chemical moieties for improved PK characteristics is likely but has not yet been reported.

We also synthesized a number of α-ketoamide inhibitors with different alkyl substituents at the α-ketoamide nitrogen. The purpose was to make these *N*-appendages reach the M^{Pro} P3′ binding pocket. Unfortunately, all these inhibitors have low *in vitro* and *in cellulo* potency. Structures of their complexes with M^{Pro} all show a *Z* configuration at the α-ketoamide. The *Z* configuration is more energetically favored than the *E* form. It is evident that steric hindrance between the hemithioacetal hydroxide and an *N*-appendage prevents the *N*-appendage from adopting a favorable position to interact with the M^{Pro} P3′ binding pocket. Although further optimization in related M^{Pro} inhibitors may likely generate interactions with the M^{Pro} P3′ binding pocket, we suggest other routes to take advantage of the M^{Pro} P3′ binding pocket. In our characterized structures, the P4 *N*-terminal isovaleramide of MPI42 shows a unique conformation that binds deep into the M^{Pro} P4 binding pocket. The *N*-terminal trifluoroacetamide of PF-07321332 binds at the same M^{Pro} pocket [14]. This unique binding explains MPI42's much higher *in vitro* potency than its close relative MPI40. We think MPI42 points to a unique way to develop potent M^{Pro} inhibitors by exploring P4 *N*-terminal chemical moieties with a similar size as isovaleramide.

4. Conclusion

Based on our systematic analysis of boceprevir-based M^{Pro} inhibitors, we conclude that a P4 *N*-terminal carbamate in an inhibitor is critical to yield high cellular and antiviral potency. However, chemical moieties at all sites including the P4 *N*-terminal carbamate and the warhead might be continuously optimized. Combined features from PF-07321332 (e.g. nitrile warhead) and newly developed inhibitors such as MPI43, MPI44 and MPI46 can be considered. In vitro DMPK and ADME assays will provide insights into how to further optimize the boceprevir-based M^{Pro} inhibitors.

Declaration of competing interest

The authors declare that they have no known competing financial interests or personal relationships that could have appeared to influence the work reported in this paper.

Data availability

Data will be made available on request.

Acknowledgement

This work was supported by Welch Foundation (grant A-1715), DHHS–NIH (R21AI164088 and R21EB032983), TAMU COS Strategic Transformative Research Program, and Texas A&M X Grants. The ALS-ENABLE beam-lines are supported in part by the National Institutes of Health, National Institute of General Medical Sciences, grant P30 GM124169-01 and the Howard Hughes Medical Institute. The Advanced Light Source is a Department of Energy Office of Science User Facility under Contract No. DE-AC02-05CH11231.

Appendix A. Supplementary data

Supplementary data to this article can be found online at https://doi.org/10.1016/j.ejmech.2022.114596.

References

[1] J.D. Baker, R.L. Uhrich, G.C. Kraemer, J.E. Love, B.C. Kraemer, A drug repurposing screen identifies hepatitis C antivirals as inhibitors of the SARS-CoV2 main protease, PLoS One 16 (2021), e0245962.

[2] J.S. Morse, T. Lalonde, S. Xu, W.R. Liu, Learning from the past: possible urgent prevention and treatment options for severe acute respiratory infections caused by 2019-nCoV, Chembiochem 21 (2020) 730–738.

[3] D.E. Gordon, G.M. Jang, M. Bouhaddou, J. Xu, K. Obernier, K.M. White, M. J. O'Meara, V.V. Rezelj, J.Z. Guo, D.L. Swaney, T.A. Tummino, R. Huttenhain, R. M. Kaake, A.L. Richards, B. Tutuncuoglu, H. Foussard, J. Batra, K. Haas, M. Modak, M. Kim, P. Haas, B.J. Polacco, H. Braberg, J.M. Fabius, M. Eckhardt, M. Soucheray, M.J. Bennett, M. Cakir, M.J. McGregor, Q. Li, B. Meyer, F. Roesch, T. Vallet, A. Mac Kain, L. Miorin, E. Moreno, Z.Z.C. Naing, Y. Zhou, S. Peng, Y. Shi, Z. Zhang, W. Shen, I.T. Kirby, J.E. Melnyk, J.S. Chorba, K. Lou, S.A. Dai, I. Barrio-Hernandez, D. Memon, C. Hernandez-Armenta, J. Lyu, C.J.P. Mathy, T. Perica, K.B. Pilla, S. J. Ganesan, D.J. Saltzberg, R. Rakesh, X. Liu, S.B. Rosenthal, L. Calviello, S. Venkataramanan, J. Liboy-Lugo, Y. Lin, X.P. Huang, Y. Liu, S.A. Wankowicz, M. Bohn, M. Safari, F.S. Ugur, C. Koh, N.S. Savar, Q.D. Tran, D. Shengjuler, S. J. Fletcher, M.C. O'Neal, Y. Cai, J.C.J. Chang, D.J. Broadhurst, S. Klippsten, P. P. Sharp, N.A. Wenzell, D. Kuzuoglu-Ozturk, H.Y. Wang, R. Trenker, J.M. Young, D. A. Cavero, J. Hiatt, T.L. Roth, U. Rathore, A. Subramanian, J. Noack, M. Hubert, R. M. Stroud, A.D. Frankel, O.S. Rosenberg, K.A. Verba, D.A. Agard, M. Ott, M. Emerman, N. Jura, M. von Zastrow, E. Verdin, A. Ashworth, O. Schwartz, C. d'Enfert, S. Mukherjee, M. Jacobson, H.S. Malik, D.G. Fujimori, T. Ideker, C. S. Craik, S.N. Floor, J.S. Fraser, J.D. Gross, A. Sali, B.L. Roth, D. Ruggero, J. Taunton, T. Kortemme, P. Beltrao, M. Vignuzzi, A. Garcia-Sastre, K.M. Shokat, B. K. Shoichet, N.J. Krogan, A SARS-CoV-2 protein interaction map reveals targets for drug repurposing, Nature 583 (2020) 459–468.

[4] A. Douangamath, D. Fearon, P. Gehrtz, T. Krojer, P. Lukacik, C.D. Owen, E. Resnick, C. Strain-Damerell, A. Aimon, P. Abranyi-Balogh, J. Brandao-Neto, A. Carbery, G. Davison, A. Dias, T.D. Downes, L. Dunnett, M. Fairhead, J.D. Firth, S. P. Jones, A. Keeley, G.M. Keseru, H.F. Klein, M.P. Martin, M.E.M. Noble, P. O'Brien, A. Powell, R.N. Reddi, R. Skyner, M. Snee, M.J. Waring, C. Wild, N. London, F. von Delft, M.A. Walsh, Crystallographic and electrophilic fragment screening of the SARS-CoV-2 main protease, Nat. Commun. 11 (2020) 5047.

[5] L. Riva, S. Yuan, X. Yin, L. Martin-Sancho, N. Matsunaga, L. Pache, S. Burgstaller-Muehlbacher, P.D. De Jesus, P. Teriete, M.V. Hull, M.W. Chang, J.F. Chan, J. Cao, V.K. Poon, K.M. Herbert, K. Cheng, T.H. Nguyen, A. Rubanov, Y. Pu, C. Nguyen, A. Choi, R. Rathnasinghe, M. Schotsaert, L. Miorin, M. Dejosez, T.P. Zwaka, K. Y. Sit, L. Martinez-Sobrido, W.C. Liu, K.M. White, M.E. Chapman, E.K. Lendy, R. J. Glynne, R. Albrecht, E. Ruppin, A.D. Mesecar, J.R. Johnson, C. Benner, R. Sun, P. G. Schultz, A.I. Su, A. Garcia-Sastre, A.K. Chatterjee, K.Y. Yuen, S.K. Chanda, Discovery of SARS-CoV-2 antiviral drugs through large-scale compound repurposing, Nature 586 (2020) 113–119.

[6] S. Gunther, P.Y.A. Reinke, Y. Fernandez-Garcia, J. Lieske, T.J. Lane, H.M. Ginn, F. H.M. Koua, C. Ehrt, W. Ewert, D. Oberthuer, O. Yefanov, S. Meier, K. Lorenzen, B. Krichel, J.D. Kopicki, L. Gelisio, W. Brehm, I. Dunkel, B. Seychell, H. Gieseler, B. Norton-Baker, B. Escudero-Perez, M. Domaracky, S. Saouane, A. Tolstikova, T. A. White, A. Hanle, M. Groessler, H. Fleckenstein, F. Trost, M. Galchenkova, Y. Gevorkov, C. Li, S. Awel, A. Peck, M. Barthelmess, F. Schlunzen, P. Lourdu Xavier, N. Werner, H. Andaleeb, N. Ullah, S. Falke, V. Srinivasan, B.A. Franca, M. Schwinzer, H. Brognaro, C. Rogers, D. Melo, J.J. Zaitseva-Doyle, J. Knoska, G. E. Pena-Murillo, A.R. Mashhour, V. Hennicke, P. Fischer, J. Hakanpaa, J. Meyer, P. Gribbon, B. Ellinger, M. Kuzikov, M. Wolf, A.R. Beccari, G. Bourenkov, D. von Stetten, G. Pompidor, I. Bento, S. Panneerselvam, I. Karpics, T.R. Schneider, M. M. Garcia-Alai, S. Niebling, C. Gunther, C. Schmidt, R. Schubert, H. Han, J. Boger, D.C.F. Monteiro, L. Zhang, X. Sun, J. Pletzer-Zelgert, J. Wollenhaupt, C.G. Feiler, M.S. Weiss, E.C. Schulz, P. Mehrabi, K. Karnicar, A. Usenik, J. Loboda, H. Tidow, A. Chari, R. Hilgenfeld, C. Uetrecht, R. Cox, A. Zaliani, T. Beck, M. Rarey, S. Gunther, D. Turk, W. Hinrichs, H.N. Chapman, A.R. Pearson, C. Betzel, A. Meents, X-ray screening identifies active site and allosteric inhibitors of SARS-CoV-2 main protease, Science 372 (2021) 642–646.

[7] M.M. Ghahremanpour, J. Tirado-Rives, M. Deshmukh, J.A. Ippolito, C.H. Zhang, I. Cabeza de Vaca, M.E. Liosi, K.S. Anderson, W.L. Jorgensen, Identification of 14 known drugs as inhibitors of the main protease of SARS-CoV-2, ACS Med. Chem. Lett. 11 (2020) 2526–2533.

[8] Z. Jin, X. Du, Y. Xu, Y. Deng, M. Liu, Y. Zhao, B. Zhang, X. Li, L. Zhang, C. Peng, Y. Duan, J. Yu, L. Wang, K. Yang, F. Liu, R. Jiang, X. Yang, T. You, X. Liu, X. Yang, F. Bai, H. Liu, X. Liu, L.W. Guddat, W. Xu, G. Xiao, C. Qin, Z. Shi, H. Jiang, Z. Rao, H. Yang, Structure of M(pro) from SARS-CoV-2 and discovery of its inhibitors, Nature 582 (2020) 289–293.

[9] Z. Jin, Y. Zhao, Y. Sun, B. Zhang, H. Wang, Y. Wu, Y. Zhu, C. Zhu, T. Hu, X. Du, Y. Duan, J. Yu, X. Yang, X. Yang, K. Yang, X. Liu, L.W. Guddat, G. Xiao, L. Zhang, H. Yang, Z. Rao, Structural basis for the inhibition of SARS-CoV-2 main protease by antineoplastic drug carmofur, Nat. Struct. Mol. Biol. 27 (2020) 529–532.

[10] Z. Li, X. Li, Y.Y. Huang, Y. Wu, R. Liu, L. Zhou, Y. Lin, D. Wu, L. Zhang, H. Liu, X. Xu, K. Yu, Y. Zhang, J. Cui, C.G. Zhan, X. Wang, H.B. Luo, Identify potent SARS-CoV-2 main protease inhibitors via accelerated free energy perturbation-based virtual screening of existing drugs, Proc. Natl. Acad. Sci. U.S.A. 117 (2020) 27381–27387.

[11] C. Ma, Y. Hu, J.A. Townsend, P.I. Lagarias, M.T. Marty, A. Kolocouris, J. Wang, Ebselen, Carmofur Disulfiram, PX-12, tideglusib, and shikonin are nonspecific promiscuous SARS-CoV-2 main protease inhibitors, ACS Pharmacol. Transl. Sci. 3 (2020) 1265–1277.

[12] E.C. Vatansever, K.S. Yang, A.K. Drelich, K.C. Kratch, C.C. Cho, K.R. Kempaiah, J. C. Hsu, D.M. Mellott, S. Xu, C.K. Tseng, W.R. Liu, Bepridil is potent against SARS-CoV-2 in vitro, Proc. Natl. Acad. Sci. U.S.A. 118 (2021), e2012201118.

[13] M. Cevik, K. Kuppalli, J. Kindrachuk, M. Peiris, Virology, transmission, and pathogenesis of SARS-CoV-2, BMJ 371 (2020) m3862.

[14] D.R. Owen, C.M.N. Allerton, A.S. Anderson, L. Aschenbrenner, M. Avery, S. Berritt, B. Boras, R.D. Cardin, A. Carlo, K.J. Coffman, A. Dantonio, L. Di, H. Eng, R. Ferre, K.S. Gajiwala, S.A. Gibson, S.E. Greasley, B.L. Hurst, E.P. Kadar, A.S. Kalgutkar, J. C. Lee, J. Lee, W. Liu, S.W. Mason, S. Noell, J.J. Novak, R.S. Obach, K. Ogilvie, N. C. Patel, M. Pettersson, D.K. Rai, M.R. Reese, M.F. Sammons, J.G. Sathish, R.S. P. Singh, C.M. Steppan, A.E. Stewart, J.B. Tuttle, L. Updyke, P.R. Verhoest, L. Wei, Q. Yang, Y. Zhu, An oral SARS-CoV-2 M(pro) inhibitor clinical candidate for the treatment of COVID-19, Science 374 (2021) 1586–1593.

[15] L. Fu, F. Ye, Y. Feng, F. Yu, Q. Wang, Y. Wu, C. Zhao, H. Sun, B. Huang, P. Niu, H. Song, Y. Shi, X. Li, W. Tan, J. Qi, G.F. Gao, Both Boceprevir and GC376 efficaciously inhibit SARS-CoV-2 by targeting its main protease, Nat. Commun. 11 (2020) 4417.

[16] C. Ma, M.D. Sacco, B. Hurst, J.A. Townsend, Y. Hu, T. Szeto, X. Zhang, B. Tarbet, M.T. Marty, Y. Chen, J. Wang, Boceprevir, GC-376, and calpain inhibitors II, XII inhibit SARS-CoV-2 viral replication by targeting the viral main protease, Cell Res. 30 (2020) 678–692.

[17] R. Oerlemans, A.J. Ruiz-Moreno, Y. Cong, N. Dinesh Kumar, M.A. Velasco-Velazquez, C.G. Neochoritis, J. Smith, F. Reggiori, M.R. Groves, A. Domling, Repurposing the HCV NS3-4A protease drug boceprevir as COVID-19 therapeutics, RSC Med. Chem. 12 (2020) 370–379.

[18] A.Y. Howe, S. Venkatraman, The discovery and development of boceprevir: a novel, first-generation inhibitor of the hepatitis C virus NS3/4A serine protease, J. Clin. Transl. Hepatol. 1 (2013) 22–32.

[19] D.W. Kneller, S. Galanie, G. Phillips, H.M. O'Neill, L. Coates, A. Kovalevsky, Malleability of the SARS-CoV-2 3CL M(pro) active-site cavity facilitates binding of clinical antivirals, Structure 28 (2020) 1313–1320 e1313.

[20] J. Qiao, Y.S. Li, R. Zeng, F.L. Liu, R.H. Luo, C. Huang, Y.F. Wang, J. Zhang, B. Quan, C. Shen, X. Mao, X. Liu, W. Sun, W. Yang, X. Ni, K. Wang, L. Xu, Z.L. Duan, Q. C. Zou, H.L. Zhang, W. Qu, Y.H. Long, M.H. Li, R.C. Yang, X. Liu, J. You, Y. Zhou, R. Yao, W.P. Li, J.M. Liu, P. Chen, Y. Liu, G.F. Lin, X. Yang, J. Zou, L. Li, Y. Hu, G. W. Lu, W.M. Li, Y.Q. Wei, Y.T. Zheng, J. Lei, S. Yang, SARS-CoV-2 M(pro) inhibitors with antiviral activity in a transgenic mouse model, Science 371 (2021) 1374–1378.

[21] W. Cao, C.D. Cho, Z.Z. Geng, N. Shaabani, X.R. Ma, E.C. Vatansever, Y. R. Alugubelli, Y. Ma, S.P. Chaki, W.H. Ellenburg, K.S. Yang, Y. Qiao, R. Allen, B. W. Neuman, H. Ji, S. Xu, W.R. Liu, Evaluation of SARS-CoV-2 main protease inhibitors using a novel cell-based assay, ACS Cent. Sci. 8 (2022) 192–204.

[22] W.R. Liu, C.A. Fierke, S. Xu, K.S. Yang, X.R. Ma, Y. Ma, Y.R. Alugubelli, E. C. Vatansever, C.-C. Cho, Z.Z. Geng, K. Khatua, SARS-CoV-2 Main Protease Inhibitors, World Intellectual Property Organization, 2021, WO2022020711A2022020711.

[23] K.S. Yang, X.R. Ma, Y. Ma, Y.R. Alugubelli, D.A. Scott, E.C. Vatansever, A. K. Drelich, B. Sankaran, Z.Z. Geng, L.R. Blankenship, H.E. Ward, Y.J. Sheng, J. C. Hsu, K.C. Kratch, B. Zhao, H.S. Hayatshahi, J. Liu, P. Li, C.A. Fierke, C.K. Tseng, S. Xu, W.R. Liu, A quick route to multiple highly potent SARS-CoV-2 main protease inhibitors, ChemMedChem 16 (2021) 942–948.

[24] W. Dai, B. Zhang, X.M. Jiang, H. Su, J. Li, Y. Zhao, X. Xie, Z. Jin, J. Peng, F. Liu, C. Li, Y. Li, F. Bai, H. Wang, X. Cheng, X. Cen, S. Hu, X. Yang, J. Wang, X. Liu, G. Xiao, H. Jiang, Z. Rao, L.K. Zhang, Y. Xu, H. Yang, H. Liu, Structure-based design of antiviral drug candidates targeting the SARS-CoV-2 main protease, Science 368 (2020) 1331–1335.

[25] L. Zhang, D. Lin, X. Sun, U. Curth, C. Drosten, L. Sauerhering, S. Becker, K. Rox, R. Hilgenfeld, Crystal structure of SARS-CoV-2 main protease provides a basis for design of improved alpha-ketoamide inhibitors, Science 368 (2020) 409–412.

[26] W. Dai, D. Jochmans, H. Xie, H. Yang, J. Li, H. Su, D. Chang, J. Wang, J. Peng, L. Zhu, Y. Nian, R. Hilgenfeld, H. Jiang, K. Chen, L. Zhang, Y. Xu, J. Neyts, H. Liu, Design, synthesis, and biological evaluation of peptidomimetic aldehydes as broad-spectrum inhibitors against enterovirus and SARS-CoV-2, J. Med. Chem. 65 (2022) 2794–2808.

[27] S. Vankadara, Y.X. Wong, B. Liu, Y.Y. See, L.H. Tan, Q.W. Tan, G. Wang, R. Karuna, X. Guo, S.T. Tan, J.Y. Fong, J. Joy, C.S.B. Chia, A head-to-head comparison of the inhibitory activities of 15 peptidomimetic SARS-CoV-2 3CLpro inhibitors, Bioorg. Med. Chem. Lett. 48 (2021), 128263.

[28] W. Vuong, C. Fischer, M.B. Khan, M.J. van Belkum, T. Lamer, K.D. Willoughby, J. Lu, E. Arutyunova, M.A. Joyce, H.A. Saffran, J.A. Shields, H.S. Young, J. A. Nieman, D.L. Tyrrell, M.J. Lemieux, J.C. Vederas, Improved SARS-CoV-2 M(pro) inhibitors based on feline antiviral drug GC376: structural enhancements, increased solubility, and micellar studies, Eur. J. Med. Chem. 222 (2021), 113584.

[29] C.H. Zhang, E.A. Stone, M. Deshmukh, J.A. Ippolito, M.M. Ghahremanpour, J. Tirado-Rives, K.A. Spasov, S. Zhang, Y. Takeo, S.N. Kudalkar, Z. Liang, F. Isaacs, B. Lindenbach, S.J. Miller, K.S. Anderson, W.L. Jorgensen, Potent noncovalent inhibitors of the main protease of SARS-CoV-2 from molecular sculpting of the drug perampanel guided by free energy perturbation calculations, ACS Cent. Sci. 7 (2021) 467–475.

[30] S. Konno, K. Kobayashi, M. Senda, Y. Funai, Y. Seki, I. Tamai, L. Schakel, K. Sakata, T. Pillaiyar, A. Taguchi, A. Taniguchi, M. Gutschow, C.E. Muller, K. Takeuchi, M. Hirohama, A. Kawaguchi, M. Kojima, T. Senda, Y. Shirasaka, W. Kamitani, Y. Hayashi, 3CL protease inhibitors with an electrophilic arylketone moiety as anti-SARS-CoV-2 agents, J. Med. Chem. 65 (2022) 2926–2939.

[31] M.D. Sacco, C. Ma, P. Lagarias, A. Gao, J.A. Townsend, X. Meng, P. Dube, X. Zhang, Y. Hu, N. Kitamura, B. Hurst, B. Tarbet, M.T. Marty, A. Kolocouris, Y. Xiang, Y. Chen, J. Wang, Structure and inhibition of the SARS-CoV-2 main protease reveal strategy for developing dual inhibitors against M(pro) and cathepsin L, Sci. Adv. 6 (2020), eabe0751.

[32] Y. Ma, K.S. Yang, Z.Z. Geng, Y.R. Alugubelli, N. Shaabani, E.C. Vatansever, R. M. Xinyu, C.-C. Cho, K. Khatua, J. Xiao, L.R. Blankenship, G. Yu, B. Sankaran, P. Li, R. Allen, H. Ji, S. Xu, W.R. Liu, A multi-pronged evaluation of aldehyde-based tripeptidyl main protease inhibitors as SARS-CoV-2 antivirals, Eur. J. Med. Chem. (2022), 2021.2012.2018.473326.

[33] K.S. Yang, X.R. Ma, Y. Ma, Y.R. Alugubelli, D.A. Scott, E.C. Vatansever, A. K. Drelich, B. Sankaran, Z.Z. Geng, L.R. Blankenship, H.E. Ward, Y.J. Sheng, J. C. Hsu, K.C. Kratch, B. Zhao, H.S. Hayatshahi, J. Liu, P. Li, C.A. Fierke, C.K. Tseng, S. Xu, W.R. Liu, A quick route to multiple highly potent SARS-CoV-2 main protease inhibitors, ChemMedChem 16 (2021) 942–948.

[34] J. Breidenbach, C. Lemke, T. Pillaiyar, L. Schakel, G. Al Hamwi, M. Diett, R. Gedschold, N. Geiger, V. Lopez, S. Mirza, V. Namasivayam, A.C. Schiedel, K. Sylvester, D. Thimm, C. Vielmuth, L. Phuong Vu, M. Zyulina, J. Bodem, M. Gutschow, C.E. Muller, Targeting the main protease of SARS-CoV-2: from the establishment of high throughput screening to the design of tailored inhibitors, Angew. Chem. Int. Ed. 60 (2021) 10423–10429.

[35] M. Westberg, Y. Su, X. Zou, L. Ning, B. Hurst, B. Tarbet, M.Z. Lin, Rational design of a new class of protease inhibitors for the potential treatment of coronavirus diseases, bioRxiv 2009 (2020) 2020, 2015.275891.

[36] C. Ma, Z. Xia, M.D. Sacco, Y. Hu, J.A. Townsend, X. Meng, J. Choza, H. Tan, J. Jang, M.V. Gongora, X. Zhang, F. Zhang, Y. Xiang, M.T. Marty, Y. Chen, J. Wang, Discovery of di- and trihaloacetamides as covalent SARS-CoV-2 main protease inhibitors with high target specificity, J. Am. Chem. Soc. 143 (2021) 20697–20709.

[37] Y. Zhao, C. Fang, Q. Zhang, R. Zhang, X. Zhao, Y. Duan, H. Wang, Y. Zhu, L. Feng, J. Zhao, M. Shao, X. Yang, L. Zhang, C. Peng, K. Yang, D. Ma, Z. Rao, H. Yang, Crystal structure of SARS-CoV-2 main protease in complex with protease inhibitor PF-07321332, Protein Cell 13 (2022) 689–693.

[38] K.S. Yang, S.Z. Leeuwon, S. Xu, W.R. Liu, Evolutionary and structural insights about potential SARS-CoV-2 evasion of nirmatrelvir, J. Med. Chem. (2022).

[39] X.R. Ma, Y.R. Alugubelli, Y. Ma, E.C. Vatansever, D.A. Scott, Y. Qiao, G. Yu, S. Xu, W.R. Liu, MPI8 is potent against SARS-CoV-2 by inhibiting dually and selectively

the SARS-CoV-2 main protease and the host cathepsin L, ChemMedChem 17 (2022), e202100456.
[40] M. Hoffmann, H. Kleine-Weber, S. Schroeder, N. Kruger, T. Herrler, S. Erichsen, T. S. Schiergens, G. Herrler, N.H. Wu, A. Nitsche, M.A. Muller, C. Drosten, S. Pohlmann, SARS-CoV-2 cell entry depends on ACE2 and TMPRSS2 and is blocked by a clinically proven protease inhibitor, Cell 181 (2020) 271–280.
[41] M.M. Zhao, W.L. Yang, F.Y. Yang, L. Zhang, W.J. Huang, W. Hou, C.F. Fan, R. H. Jin, Y.M. Feng, Y.C. Wang, J.K. Yang, Cathepsin L plays a key role in SARS-CoV-2 infection in humans and humanized mice and is a promising target for new drug development, Signal Transduct. Targeted Ther. 6 (2021) 134.
[42] Y.W. Cheng, T.L. Chao, C.L. Li, M.F. Chiu, H.C. Kao, S.H. Wang, Y.H. Pang, C. H. Lin, Y.M. Tsai, W.H. Lee, M.H. Tao, T.C. Ho, P.Y. Wu, L.T. Jang, P.J. Chen, S. Y. Chang, S.H. Yeh, Furin inhibitors block SARS-CoV-2 spike protein cleavage to suppress virus production and cytopathic effects, Cell Rep. 33 (2020), 108254.
[43] P. Kumar, A. Nagarajan, P.D. Uchil, Analysis of cell viability by the MTT assay, Cold Spring Harb. Protoc. 2018 (2018) 469–471.
[44] Y. Wang, H. Xie, Y.R. Alugubelli, Y. Ma, S. Xu, J. Ma, W.R. Liu, D. Liang, Accurate mass identification of an interfering water adduct and strategies in development and validation of an LC-MS/MS method for quantification of MPI8, a potent SARS-CoV-2 main protease inhibitor, in: Rat Plasma in Pharmacokinetic Studies, Pharmaceuticals (Basel), vol. 15, 2022, p. 676.
[45] M.S. Sulkowski, D.L. Thomas, R.E. Chaisson, R.D. Moore, Hepatotoxicity associated with antiretroviral therapy in adults infected with human immunodeficiency virus and the role of hepatitis C or B virus infection, JAMA 283 (2000) 74–80.
[46] P. Tebas, W.G. Powderly, S. Claxton, D. Marin, W. Tantisiriwat, S.L. Teitelbaum, K. E. Yarasheski, Accelerated bone mineral loss in HIV-infected patients receiving potent antiretroviral therapy, AIDS 14 (2000) F63–F67.
[47] D. Nolan, P. Reiss, S. Mallal, Adverse effects of antiretroviral therapy for HIV infection: a review of selected topics, Expet Opin. Drug Saf. 4 (2005) 201–218.
[48] J.A. Henry, I.R. Hill, Fatal interaction between ritonavir and MDMA, Lancet 352 (1998) 1751–1752.
[49] Z. Mansuri, B. Shah, M. Adnan, G. Chaudhari, T. Jolly, Ritonavir/Lopinavir and its Potential Interactions with Psychiatric Medications: A COVID-19 Perspective, Prim, vol. 22, Care Companion CNS Disord., 2020, 20com02677.